RSC Advances

PAPER

View Article Online
View Journal | View Issue

Cite this: *RSC Adv.*, 2023, **13**, 24944

Performance investigation of $LiCl \cdot H_2O$-γ-Al_2O_3 composite materials for low-grade heat storage

Lin Li, [ac] Tao Zeng, *[ab] Hongyu Huang, [a] Jun Li,[a] Noriyuki Kobayshi[d] and Xiaohu Yang*[b]

In this study, the influences of nano γ-Al_2O_3 on the thermal storage performance of LiCl were experimentally investigated. The XRD results show that a complex of lithium aluminium oxychloride ($LiAlOCl_2$) was formed through the $LiCl \cdot H_2O$ and γ-Al_2O_3 composites preparation process. The *in situ* diffuse reflectance infrared Fourier transform spectroscopy measurement reveals that the addition of γ-Al_2O_3 accelerated the hydration rate of LiCl composites, concentrated the spectrum utilization range, and promoted the desorption rate of physical adsorbed H_2O and low-frequency structural –OH in the materials. The highest specific surface area of the composite is 34.5 times higher than that of pure LiCl. The addition of γ-Al_2O_3 can increase the conversion rate of $LiCl \cdot H_2O$ to approximately 100% at the hydration time of 1 h and the addition content of γ-Al_2O_3 at 15 wt%. A maximum heat storage density (HSD) for the $LiCl \cdot H_2O$-γ-Al_2O_3 composite can reach 714.7 kJ $kg_{LiCl \cdot H_2O}^{-1}$ in 1 h when the addition content of γ-Al_2O_3 was 15%$_{wt}$ and its water uptake can reach 0.26 g g^{-1} in 1 h. It also can be found that the addition of Al_2O_3 in LiCl resulted in a decrease of the activation energy from 90.89 kJ mol^{-1} to 79.76 kJ mol^{-1}. However, the thermal conductivity of the $LiCl \cdot H_2O$-γ-Al_2O_3 composite slightly decreased with the increase of nano γ-Al_2O_3 content.

Received 8th June 2023
Accepted 14th August 2023

DOI: 10.1039/d3ra03835a

rsc.li/rsc-advances

1 Introduction

Plenty of waste heat, about 66% being low-grade heat (below 200 °C), is discharged into the environment directly during industrial processes.[1,2] Therefore, the efficient use of low-grade waste heat can reduce energy consumption, which has been attracting much attention during recent decades.[3–5] Unfortunately, low-grade waste heat is difficult to recover and utilize due to its low exergy.[6] Thermal energy storage (TES) technologies are some of the most hopeful methods for realizing continuous and stable utilization of waste heat,[7] which is classified into three types: sensible,[8,9] latent[10,11] and thermochemical heat storage (TCS).[12–14] TCS utilizing reversible chemical reactions to store and release energy with high HSD[15–17] and lossless heat storage[18] makes a promising and useful contribution to the storage of low-grade thermal energy. Various TCS materials have been studied, such as metal salts with water,[19,20] ammonia,[21–23] methanol,[24,25] or metal alloys with hydrogen.[26,27] In a relevant research article, Cot-Gores *et al.* reported that water as an environmentally friendly adsorbate could meet the requirements of safety system, and crystalline hydrate as a heat storage material had a good development prospect.[28] Hygroscopic salts like LiCl, LiBr, KBr, and $CaCl_2$ can be used as suitable heat storage materials.[29]

Lithium chloride hydrate ($LiCl \cdot nH_2O$) was selected as a promising candidate for low-grade heat storage.[30] The reversible chemical reaction[31] for LiCl at normal temperatures and pressures is as follows:

$$LiCl \cdot H_2O(s) \leftrightarrow LiCl(s) + H_2O(g) \quad (1)$$

The deliquescence relative humidity (DRH) value for LiCl at 30 °C is 11%. The complete water absorption process of inorganic salts can be considered as a three-phase process involving chemisorption (mainly energy storage part), gas/liquid/solid three-phase liquid hydrolysis/crystallization, liquid/gas absorption and other processes. Most scholars mainly pay attention to the total amount of water vapor adsorption of hygroscopic salt materials to increase the HSD,[32–34] but rarely pay attention to the adsorption amount per unit time (sorption kinetics) on materials' use. In some industrial waste heat recycle, a large amount of waste heat needs to be treated or recovered promptly. For the short-term TCS, the proportion of chemical heat storage should be enhanced to increase the HSD

[a]*Guangzhou Institute of Energy Conversion, Chinese Academy of Sciences, Guangzhou 510640, China. E-mail: zengtao@ms.giec.ac.cn*

[b]*Science and Technology in Thermal Energy and Power Laboratory, Wuhan Second Ship Design and Research Institute, Wuhan 430205, China. E-mail: yangxhcsic@163.com*

[c]*University of Chinese Academy of Sciences, Beijing 100049, China*

[d]*Department of Chemical Systems Engineering, Nagoya University, Nagoya 464-8603, Japan*

per unit time.[35] To improve the sorption kinetics and solve limitations (deliquescence and agglomeration) of LiCl, composites are usually advanced by adding porous media with high specific surface area to increase the contact abilities with water.[30,36–39] Zhao *et al.* modified LiCl with zeolite, and the water uptake capacity within 1 h was less than 0.15 g g^{-1} at 25 °C and 80% RH.[40] Zhang *et al.* chose activated alumina spherical grain (3.29–5.30 mm) as the matrix and LiCl as the inserted salt and the maximum water uptake capacity within 1 h was about 0.2 g g^{-1} at 20 °C and 80% RH and its adsorption capacity per unit time has been greatly improved compared with other materials.[41] Existing studies mainly focus on the thermochemical characterizations of the prepared composite materials, there is a lack of further theoretical analyses and in-depth study on the reaction kinetics of hydration and dehydration process, which is of exceptional importance for deeper understanding of the heat storage mechanism. Moreover, to motivate advancement of TCE in the field short-term energy storage, the sorption performances of composite materials must be further improved. Powdered nano aluminum oxide (Al_2O_3) attracts the attention of many scholars to choose it to selective adsorption for gases, water vapor and water in some liquids as the additive due to its high porosity, high activity, and low cost.[42–46] And it was also proven that a small amount of transition metals and their oxides have a large effect on the thermodynamic properties of MgH_2 (ref. 47) and the cations had a strong influence on the hydration energy.[48–50]

To further improve the water sorption kinetics of materials for short-term TCS, this paper selected powdered nano γ-Al_2O_3 as the additive which can increase the contact opportunities and binding capacity with water, and the proportion of LiCl is greatly increased to strengthen the hydration reactants. The structure and properties of LiCl-γ-Al_2O_3 TCS composites were analyzed by *in situ* diffuse reflectance infrared Fourier transform (DRIFT) spectroscopy, X-ray diffraction (XRD), and other micro characterization methods. Then, a further study on how γ-Al_2O_3 affected the sorption kinetics and thermal storage performance of LiCl from the aspect of reaction mechanism was investigated.

2 Experimental methods

2.1 Materials and preparation procedure

All the raw materials are purchased from Aladdin Reagent Co., Ltd. The LiCl (purity, >99.99%) was used as hydrated salt. Nano γ-Al_2O_3 (purity, >99.9%) was selected as the porous matrix. Fig. 1 schematically illustrates the preparation process of LiCl-γ-Al_2O_3 composites. Firstly, pretreat LiCl and γ-Al_2O_3 with an oven at 100 °C for 2 h and prepare four LiCl solutions which concentration are 10% and volume is 90 ml respectively. Then different mass (526.3 mg, 1111.1 mg, 1764.7 mg, 2500 mg) of γ-Al_2O_3 was impregnated with the LiCl solution at a stirring rate of 600 rpm for 12 h to form the composite solution. Finally, the composite solutions were dried at 100 °C for 12 h, and then at 200 °C for 6 h in the oven, to obtain the anhydrous composites (LiCl-Al_2O_3). The hydrous composites (LiCl·H_2O-Al_2O_3) were acquired by the hydration of the anhydrous composites in a constant temperature and humidity chamber (Labonce-60CH, ±0.5 °C, ±3% RH) at 30 °C and 60% RH. The masses were measured by an analytical balance (MS105DU, Mettler-Toledo, ±0.01 mg). The resulting materials were sequentially named LiCl·H_2O-Al_2O_3-5%, LiCl·H_2O-Al_2O_3-10%, LiCl·H_2O-Al_2O_3-15% and LiCl·H_2O-Al_2O_3-20%.

2.2 Characterization and thermal storage performance evaluation of composites

The transmission electron micrographs (TEM) equipped with a FEI Tecnai G212 and a JEOL JEM-2100F was used to record microstructure pictures. The crystal structures of the samples were analyzed and obtained on a D8-advance X-ray diffractometer with a scanning step of 0.0167° and counting time of 10.160 s per step. The thermal conductivity was measured by a hot disk thermal constant analyzer (TPS 500 (S), Hot Disk AB Company, Sweden, ±5%). The Brunauer–Emmett–Teller (BET) specific surface area and pore volume were evaluated by the nitrogen physical adsorption method with the Quantachrome QDS-30 analyzer (±1%). After obtaining hydrates, the thermogravimetric and differential thermal analyzer (TG-DSC, STA-200, Nanjingdazhan, ±0.1 °C) was used to measure the

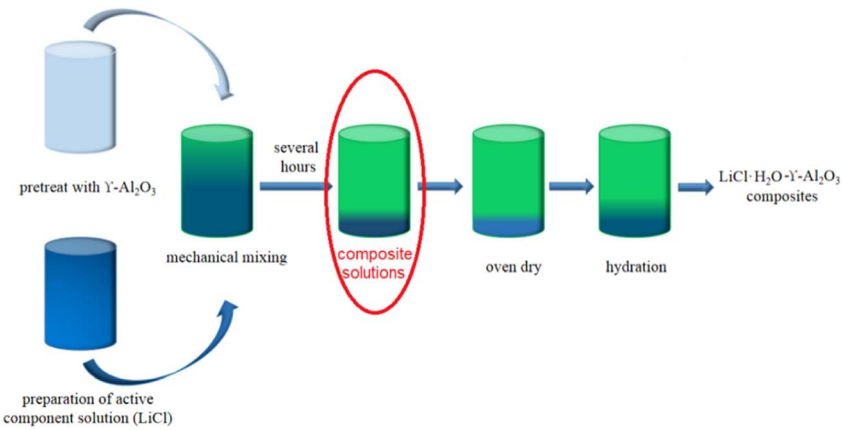

Fig. 1 Preparation flow chart of LiCl-γ-Al_2O_3 composites.

endothermic heat and weight change during the dehydration step. The TG-DSC curves were described by heating the samples from 30 °C to 200 °C at the heating rate of 10 °C min^{-1} under the nitrogen atmosphere.

The uncertainty of the composite content was mainly caused by the mass measurements of the LiCl and Al_2O_3. Therefore, the content of LiCl in composite (z) is calculated from:

$$u_z = \sqrt{\left(\frac{\partial z}{\partial m_1}u_1\right)^2 + \left(\frac{\partial z}{\partial m_2}u_2\right)^2} \quad (2)$$

where, the masses of LiCl and Al_2O_3 are respectively denoted as m_1 and m_2; u_1 and u_2 are the uncertainties associated with m_1 and m_2, respectively. The accuracy of the electronic balance is ±0.01 mg. Therefore, the uncertainties of the composite content of 95%, 90%, 85%, 80% are ±0.00045%, ±0.00041%, ±0.00037%, and ±0.00033%, respectively.

The uncertainty analysis of the hydration conversion of LiCl (α_{LiCl}) can be evaluated by the following equation.

$$u_\alpha = \sqrt{\left(\frac{\partial \alpha}{\partial w}u_w\right)^2 + \left(\frac{\partial \alpha}{\partial z}u_z\right)^2} \quad (3)$$

where u_w is the uncertainty of the relative mass change (w) measurement. The accuracies of the electronic balance in TG-DSC, is ±0.01 mg. Finally, the uncertainty of α_{LiCl} is about 1.11–1.61%.

2.3 Presentation of *in situ* DRIFT spectroscopy

KBr (99.99% spectroscopy grade), obtained from Aladdin Reagent Co., Ltd, was used as the background material and was dried at 200 °C for 6 h before testing. The effect of nano γ-Al_2O_3 on the hydration/dehydration reaction of LiCl·H_2O in a quasi environmental state was studied by *in situ* DRIFT spectroscopy Nicolet 6700 and thermogravimetric analysis of TA tgaq50, USA. Prior to the acquisition of *in situ* DRIFT spectra, pure LiCl and the LiCl-γ-Al_2O_3 composites were dried at 200 °C for 8 h in the oven, and the reactor was purged with N_2 for 20 min. Then, the samples were placed in the *in situ* reactor immediately. The reactor was purged using an N_2 flow with water vapor (100 ml min^{-1}). The condition for hydration was at 26 °C and around 60% RH. After the hydration reaction, the LiCl·H_2O was heated at a rate of 10 °C min^{-1} under the control of temperature-programmed technology with a dry N_2 flow.

3 Results and discussion

XRD patterns of pure LiCl and LiCl·H_2O-Al_2O_3 composites were recorded at room temperature as shown in Fig. 2. Diffraction peaks at around 23.08°, 32.97°, 34.97°, 40.71°, 47.46° and 58.67° are attributed to LiCl·H_2O, while peaks at 30.18°, 34.97°, 50.24°, 54.51° and 59.12° belong to $LiAlOCl_2$, a complex formed by LiCl·H_2O and γ-Al_2O_3.[51] In the XRD pattern of the composites, even if the mass fraction of γ-Al_2O_3 is as high as 20%, there is no corresponding peak of γ-Al_2O_3. This indicates that Li^+ with small radius is likely to enter into the lattice of γ-Al_2O_3 and react in bulk.[50] Both LiCl and Al_2O_3 are Lewis acids. In the process of obtaining dehydrated composite materials by impregnation, the following equation mainly occurs:

$$LiCl\cdot H_2O(s) \rightarrow LiCl(s) + H_2O(g) \quad (4)$$

However, in the process of heating, hydrolysis will also occur,[52] as follows:

$$LiCl\cdot H_2O(s) \rightarrow LiOH(s) + HCl(g) \quad (5)$$

Al_2O_3 is an amphoteric substance which can react both with base (LiOH) or acid (HCl).

$$6LiOH + Al_2O_3 \rightarrow 2Al(OH)_3 + 3Li_2O \quad (6)$$

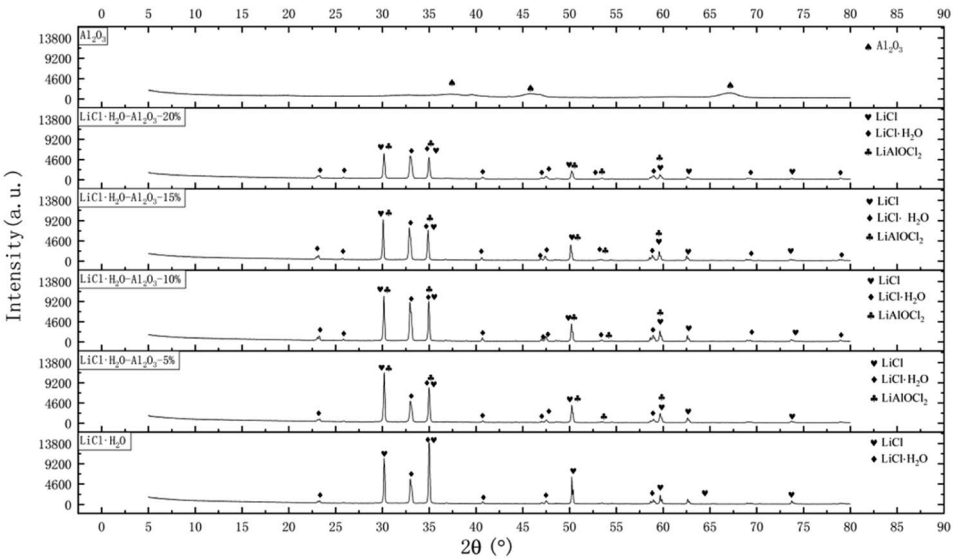

Fig. 2 XRD patterns of pure LiCl·H_2O, γ-Al_2O_3, LiCl·H_2O-Al_2O_3-5%, LiCl·H_2O-Al_2O_3-10%, LiCl·H_2O-Al_2O_3-15%, LiCl·H_2O-Al_2O_3-20% samples with different nano γ-Al_2O_3 contents.

$$6HCl + Al_2O_3 \rightarrow 2AlCl_3 + 3H_2O \quad (7)$$

Meanwhile, HCl can react with $Al(OH)_3$ as follows.

$$6HCl + 2Al(OH)_3 \rightarrow 2AlCl_3 + 3H_2O \quad (8)$$

At this time, LiCl and $AlCl_3$ may form composite salt $LiAlCl_4$.[53]

$$AlCl_3 + LiCl \rightarrow LiAlCl_4 \quad (9)$$

Then, $LiAlOCl_2$ may be generated by the following equation:[51]

$$Li_2O + LiAlCl_4 \rightarrow LiAlOCl_2 + 2LiCl \quad (10)$$

Compared to the XRD patterns of pure LiCl, there was a clear reduction of the relative intensity of the Bragg diffraction peaks at ambient temperature with the increase of γ-Al_2O_3 content. In addition, there are many diffraction peaks of $LiCl \cdot H_2O$ in the composites, which are 25.87°, 47.02°, 68.99°, and 78.94° respectively. It is speculated that –AlCl bond is formed after the reaction of LiCl with γ-Al_2O_3, which reduces the activation energy of hydration reaction.[54] It can be seen from XRD patterns that the diffraction intensity become lower and the diffraction peak range become wider. According to Scherrer formula, the reason for the above phenomenon may be that the addition of γ-Al_2O_3 provides more loading area for LiCl, so that LiCl can absorb more water vapor in the same test environment and time, resulting in the decrease of diffraction intensity; and the other reason is that the particles size of the composites become smaller and more dispersed than that of pure LiCl which can be seen in the TEM images.

The TEM images of pure LiCl, $LiCl \cdot H_2O$-Al_2O_3-5%, $LiCl \cdot H_2O$-Al_2O_3-10%, $LiCl \cdot H_2O$-Al_2O_3-15%, and $LiCl \cdot H_2O$-Al_2O_3-20% are shown in Fig. 3a–j. It can be seen that after contacting with water vapor during the TEM experiment, the pure LiCl generates agglomeration as a whole shown in Fig. 3a with strip crystal structure (about 7.3 nm, the blue part in Fig. 3b). This is due to the rapid reaction of LiCl with water vapor in the air during the preparation process before the test. When TEM shooting, there will be small moving layers (about 30 nm, the red part in Fig. 3b) on the edge and surface of the sheet structure, and the small moving layers and strip crystal structure will be significantly reduced after adding γ-Al_2O_3 (Fig. 3c–j). In addition, it can be found that with the increase of γ-Al_2O_3 content, the transparency of TEM images increases gradually which is mainly because the distribution of Al_2O_3 becomes uniform. When the content of γ-Al_2O_3 reaches 20% (Fig. 3i and j), the average particle size of γ-Al_2O_3 nanoparticles can be reduced to around 11.07 nm, and the distribution of Al_2O_3 is more consistent than that observed in Fig. 3c–h (with lower γ-Al_2O_3 content).

The SEM images of pure LiCl and $LiCl \cdot H_2O$-Al_2O_3-20% are shown in Fig. 3k and l. The pure LiCl generates agglomeration as a whole (≫ 500 μm) shown in Fig. 3k. While the particles size range of $LiCl \cdot H_2O$-Al_2O_3-20% is 2.5–10 μm which is much smaller than that of pure LiCl. In summary, the results show that the increase of γ-Al_2O_3 content is beneficial to the

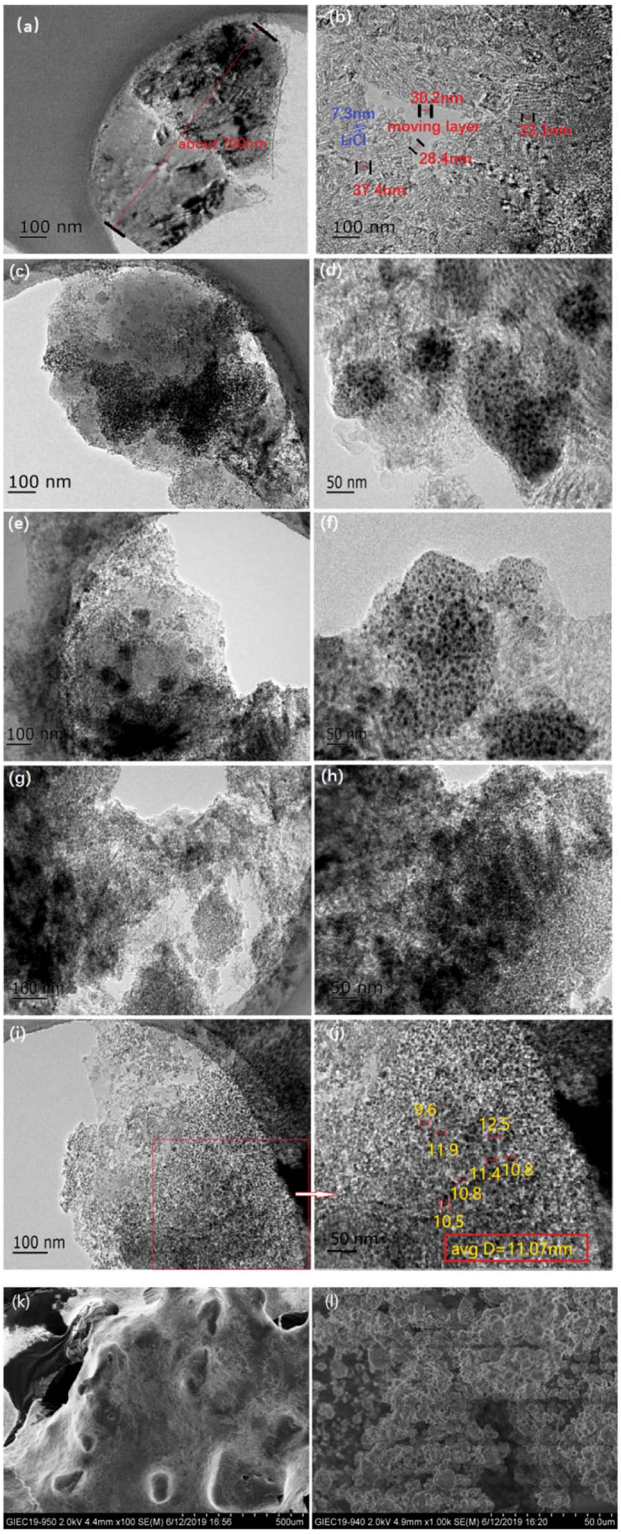

Fig. 3 TEM images of samples: (a and b) pure LiCl; (c and d) $LiCl \cdot H_2O$-Al_2O_3-5%, (e and f) $LiCl \cdot H_2O$-Al_2O_3-10%; (g and h) $LiCl \cdot H_2O$-Al_2O_3-15%; (i and j) $LiCl \cdot H_2O$-Al_2O_3-20% with different nano γ-Al_2O_3 contents; SEM images of samples; (k) pure $LiCl \cdot H_2O$; (l) $LiCl \cdot H_2O$-Al_2O_3-20%.

dispersion of LiCl, effectively inhibit the agglomeration of LiCl and $LiCl \cdot H_2O$, and facilitate the hydration process.

Fig. 4 can be used to observe the whole process of hydration and dehydration of pure $LiCl \cdot H_2O$ and composites. The *in situ* DRIFT spectroscopy of the hydration reaction of LiCl and H_2O are showed in Fig. 4a. The materials were dried at 200 °C for 8 h in the oven before hydration, while the weak peaks standing for structural –OH and physical adsorbed H_2O can be observed in Fig. 4a, demonstrating that the materials partially hydrated during the sample placement due to the hygroscopic property of LiCl. The stretching vibrations of structural –OH and physical adsorbed H_2O always assign to the bands in the range of 3800–2200 cm^{-1}.[50] The bands at 3630–2950 cm^{-1} and at 1700–1580 cm^{-1} which the peak was centered at around 1673 cm^{-1} in the spectra can be respectively attributed to the stretching vibrations ($\nu_{OH\text{-}s}$) and bending vibrations ($\beta_{OH\text{-}s}$) of the structural –OH in $LiCl \cdot H_2O$.[54,55] Moreover, the broad peak in the 3423–2842 cm^{-1} range centered around 3400 cm^{-1} and the peak at 1640 cm^{-1}, respectively, belonged to the stretching vibrations ($\nu_{OH\text{-}p}$) and bending vibrations ($\beta_{OH\text{-}p}$) of the physical adsorbed H_2O. The band between $\nu_{OH\text{-}p}$ and $\beta_{OH\text{-}p}$ (2500–1900 cm^{-1} centered at 2125 cm^{-1}) was called the sum frequency absorption H_2O band.[50,54] As the hydration reaction proceeds, the bandwidth of $\nu_{OH\text{-}s}$ markedly increased from 10 min to 70 min, indicating the continuous reaction of LiCl and H_2O after 70 min, the hydration reaction rate gradually decreased. In addition, it can be observed that the peak intensities of $\beta_{OH\text{-}s}$ gradually decreased while the $\beta_{OH\text{-}p}$ gradually appeared due to the deliquescence of LiCl. At the same time, the sum frequency absorption H_2O band gradually became wider.

Fig. 4b shows the dehydration reaction process of $LiCl \cdot H_2O$ obtained from 1.5 h hydration of LiCl *in situ* DRIFT spectroscopy reactor. Because the reactor required a certain time to reach the set temperature, the ending and initial curves in Fig. 4a and b are slightly different. When heated above 75 °C, the $\nu_{OH\text{-}s}$ was getting narrower and the peak intensities of $\beta_{OH\text{-}s}$ started to rise and the trend became more evident over 100 °C. With the increase of temperature, structural –OH and physical adsorbed H_2O gradually disappeared.

Fig. 4c shows the hydration reaction process of $LiCl\text{-}Al_2O_3$-10% and H_2O *in situ* DRIFT spectroscopy reactor. The $\nu_{OH\text{-}s}$ bands showed an obvious broadening to 3630–2950 cm^{-1} within 10 min hydration because of the existing metal coordination bond (Al^{3+}), which formed the complex compound $LiAlOCl_2$. It took 40 min that the $\nu_{OH\text{-}s}$ bands were virtually no longer wider, shorter than that of pure LiCl (70 min), indicating that the nano $\gamma\text{-}Al_2O_3$ addition enhanced the hydration reaction rate of LiCl.

Fig. 4d presents the *in situ* DRIFT spectroscopy of dehydration reaction of $LiCl \cdot H_2O\text{-}Al_2O_3$-10%. When $LiCl \cdot H_2O\text{-}Al_2O_3$-10% was heated over 75 °C, the peak intensities of $\nu_{OH\text{-}s}$ and $\beta_{OH\text{-}s}$ became sharper and narrower; beyond 125 °C, the dehydration of the composite gradually slowed down. The hydrogen bonding with Al^{3+} on the surface of $\gamma\text{-}Al_2O_3$ started to

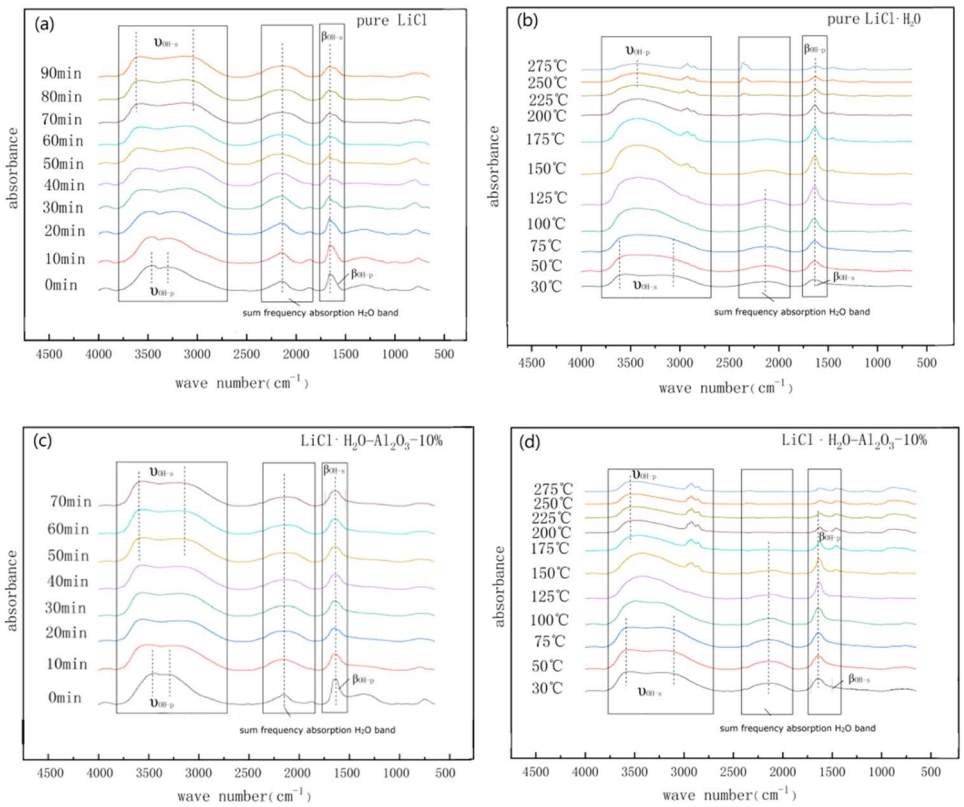

Fig. 4 The *in situ* DRIFT spectroscopy of (a) the hydration reaction of LiCl; (b) dehydration reaction of $LiCl \cdot H_2O$; (c) hydration reaction of $LiCl \cdot H_2O\text{-}Al_2O_3$-10%; (d) dehydration reaction of $LiCl \cdot H_2O\text{-}Al_2O_3$-10%.

decompose. The peak intensities of –OH in structural H_2O did not change until 175 °C, which was lower than that of pure LiCl·H_2O (225 °C). It can be found that the addition of γ-Al_2O_3 accelerated the hydration rate of LiCl, concentrated the utilization range of the spectrum, and promoted the desorption rate of physical adsorbed H_2O and low-frequency structural –OH in the materials that are consistent with our XRD data. The main reason is that the addition of Al^{3+} can enhance the stretching vibration of structural –OH (3630–2950 cm^{-1}), lead to the formation of coordination bonds between structural –OH and metal ions and promote the formation of intermolecular hydrogen bonds that further strengthens the binding of water molecules.[50,51]

The nitrogen adsorption isotherms and pore size distributions of LiCl·H_2O-Al_2O_3-5%, LiCl·H_2O-Al_2O_3-10%, LiCl·H_2O-Al_2O_3-15% and LiCl·H_2O-Al_2O_3-20% were carried out by the nitrogen adsorption method and shown in Fig. 5. It can be seen from Fig. 5a that in the low pressure region ($p/p_0 < 0.2$), there is a weak interaction between the adsorbate and the pore wall, and the adsorption curve rises slowly. With the increase of relative pressure, that is, when $0.2 < p/p_0 < 1$, the adsorption curve rises gradually. This is a typical type III adsorption isotherm, indicating that the pores are mainly mesoporous. With the increase of Al_2O_3 concentration, the increasing range of adsorption curve will be higher, and the hysteresis loop appears, which is due to the occurrence of mesoporous capillary condensation in the adsorption process, resulting in irreversible desorption process. This is a typical isotherm of type III combined with type V. In addition, a small amount of micropores gradually appear with the increase of the proportion of Al_2O_3. According to Fig. 5b, avery small amount of 5–10 nm pores were present in the pure LiCl which may result from the stacking or the voids between of LiCl particles. However, the cumulative pore volume of pure LiCl can be ignored as compared to the γ-Al_2O_3, as indicated in Table 1. In contrast, the pore size distribution of LiCl-Al_2O_3 changed significantly (Fig. 5c) and mainly concentrated within 8–15 nm, which indicated that the addition of nano γ-Al_2O_3 formed a large number of nano-scale pores. As shown in Table 1, the specific surface area of pure LiCl is low (0.4 $m^2\ g^{-1}$), and the biggest specific surface area (15.18 $m^2\ g^{-1}$) of the composite (LiCl·H_2O-Al_2O_3-20%) is 34.5 times higher than that of pure LiCl and the specific surface area (calculated by BET method), the pore volume and their proportion (microporous and mesoporous ratio) of the composites increase with the increase of the ratio of Al_2O_3. However, it has been pointed out that the mechanical mixing of additive (nano γ-Al_2O_3) and reactive salt (LiCl) could also lead to a increase of BET surface area compared to the reactive salt, due to the relatively high specific surface area of the additive.[56] For the purpose of assess the real change of surface area caused by the addition of nano γ-Al_2O_3, it is proposed that the surface area should be normalized relative to the additive weight in the composite rather than the composite weight. The normalized surface (NSA) was defined as:

$$\mathrm{NAS} = \frac{\mathrm{SA}_{\mathrm{LiCl/Al_2O_3\ composite}}}{1-z} \cdot \frac{1}{\mathrm{SA}_{\mathrm{Al_2O_3}}} \qquad (11)$$

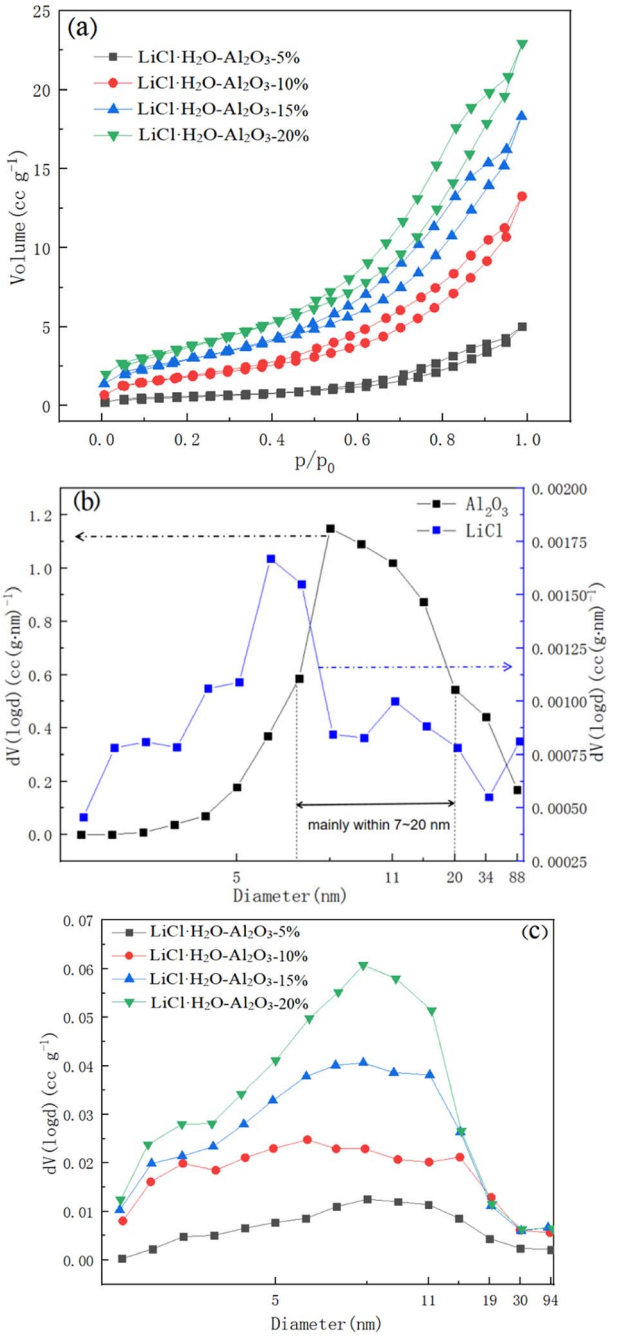

Fig. 5 (a) Nitrogen adsorption isotherms of LiCl·H_2O-Al_2O_3-5%, LiCl·H_2O-Al_2O_3-10%, LiCl·H_2O-Al_2O_3-15%, LiCl·H_2O-Al_2O_3-20%; pore size distributions of; (b) LiCl and Al_2O_3; (c) LiCl·H_2O-Al_2O_3-5%, LiCl·H_2O-Al_2O_3-10%, LiCl·H_2O-Al_2O_3-15%, LiCl·H_2O-Al_2O_3-20%.

where SA is the specific surface area of the parent Al_2O_3 or LiCl-Al_2O_3 composite, z is the percentage of LiCl content in composites, which is 95%, 90%, 85%, 80% for LiCl·H_2O-Al_2O_3-5%, LiCl·H_2O-Al_2O_3-10%, LiCl·H_2O-Al_2O_3-15%, LiCl·H_2O-Al_2O_3-20%, respectively. Thus the NAS for LiCl·H_2O-Al_2O_3-5%, LiCl·H_2O-Al_2O_3-10%, LiCl·H_2O-Al_2O_3-15%, LiCl·H_2O-Al_2O_3-20% is 0.25, 0.38, 0.40, 0.43. It can be found that the NSA of composites increases with the increase of Al_2O_3 content, which is consistent with the changes of BET surface area and pore

Table 1 Texture parameters of pure LiCl and composites with different nano γ-Al_2O_3 contents

Samples	BET Surface area (m^2 g^{-1})	Pore volume (cc g^{-1})	Average pore size (nm)
γ-Al_2O_3	176.3	0.7	15.8
LiCl·H_2O-Al_2O_3-20%	15.2	0.04	10.1
LiCl·H_2O-Al_2O_3-15%	10.7	0.03	10.6
LiCl·H_2O-Al_2O_3-10%	6.8	0.02	12.1
LiCl·H_2O-Al_2O_3-5%	2.2	0.009	14.2
Pure LiCl	0.4	0.001	12.6

volume as shown in Table 1. However, all of these values are much less than 1, indicating that LiCl particles with the size less than the pore diameter are at least partially located inside the pore while substantial pore blocking by large LiCl particles (whose sizes are comparable or higher than Al_2O_3 pore diameter) exist.[56,57]

The thermal storage performance and reaction mechanism of LiCl chemical thermal storage materials were studied by TG-DSC curve. The calculation quality of material HSD is based on the quality after material hydration. Fig. 6 is the TG-DSC curve of LiCl·H_2O-Al_2O_3 composites, which have been hydrated for 1 h at 30 °C and 60% RH. The hydration conversion of LiCl (α_{LiCl}) was calculated according to the relative mass change (w) and the percentage of LiCl content in composites (z). The calculation formula is as followed:

$$\alpha_{LiCl} = \frac{42.39(1-w)}{18wz} \times 100\% \quad (12)$$

Due to the slow hydration rate of pure LiCl, only 51.70% of LiCl is hydrated after 1 h and its HSD is only about 402.04 kJ kg^{-1} (Fig. 6a). Compared with the pure LiCl, the LiCl conversion in composites can achieve 78.28%, 82.63% and 97.34% after 1 h hydration corresponding to LiCl·H_2O-Al_2O_3-5%, LiCl·H_2O-Al_2O_3-10% and LiCl·H_2O-Al_2O_3-15% respectively, demonstrating that nano γ-Al_2O_3 is beneficial to enhance the LiCl hydration reaction rate. By changing the content of nano γ-Al_2O_3, the overall HSD of composites can reach 565.75 kJ kg^{-1} (5%), 577.75 kJ kg^{-1} (10%), and 607.5 kJ kg^{-1} (15%) respectively, and the highest HSD of LiCl·H_2O monomer can be increased to 714.7 kJ kg^{-1} (LiCl·H_2O-Al_2O_3-15%). Table 2 shows the comparison of water uptake amount for 1 h of the prepared composite with other reported composites for TCS. It can be found that the water uptake amount of composite prepared in this work can reach 0.26 g g^{-1} after 1 h hydration, exhibiting superior performance compared to other composites. Therefore, although some pores of Al_2O_3 are blocked by LiCl particles as discussed above, the hydration performance of reactive salt is improved by the addition of Al_2O_3.

Meanwhile, the decomposition temperature of composites were reduced compared with that of the pure material. There are two possible reasons why the hydration rate and HSD of LiCl·H_2O-Al_2O_3 composites have been greatly increased. First, the addition of Al^{3+} forms coordination bonds between structural –OH and metal ions and forms more intermolecular hydrogen bonds, further strengthening the binding of water molecules and enhancing the adsorption capacity of materials on water molecules to improve the hydration reaction rate. Second, when nano γ-Al_2O_3 compounded with LiCl·H_2O, the size of LiCl·H_2O particles reaches nano-scale and the surface atomic quantity increases significantly.[59]

Fig. 7 illustrates the thermal conductivity (on left-hand side) and HSD (for 1 h hydration on right-hand side) of pure LiCl and LiCl-γ-Al_2O_3 composites after a drying period of 8 h at 200 °C. It can be seen from Fig. 7 that the thermal conductivity decreases

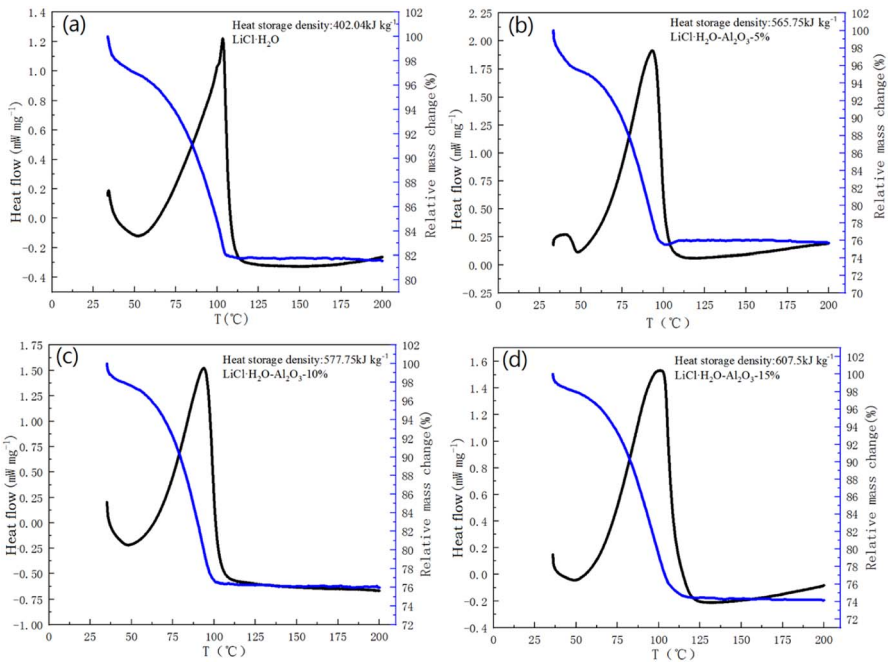

Fig. 6 TG-DSC curves of: (a) LiCl·H_2O; (b) LiCl·H_2O-Al_2O_3-5%; (c) LiCl·H_2O-Al_2O_3-10%; (d) LiCl·H_2O-Al_2O_3-15%.

Table 2 Comparison of water uptake capacity at 1 h hydration between the prepared composite and composites from literature

Composite	LiCl (or LiOH) content [%]	Temperature (°C)	Relative humidity (%)	Water uptake value (g g^{-1})
LiCl/ENG-TSA/silica[32]	33.3%$_{LiCl}$	30	60	0.14
LiCl/zeolite[40]	47.1%$_{LiCl}$	25	80	0.15
LiCl/alumina spherical grain[46]	14.7%$_{LiCl}$	20	80	0.20
LiCl/HKUST-1 (ref. 58)	52.4%$_{LiCl}$	35	50	0.21
This study	85.0%$_{LiCl}$	30	60	0.26

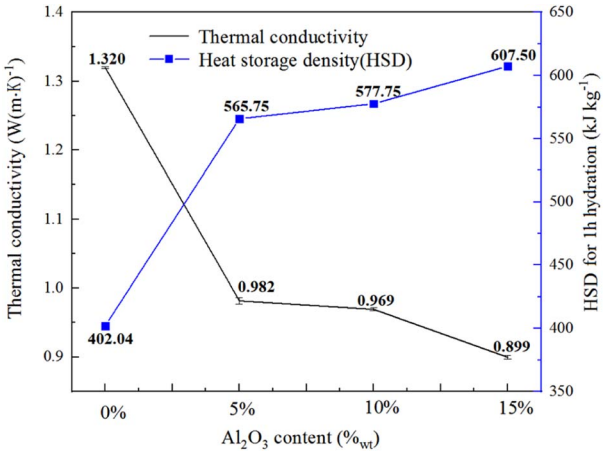

Fig. 7 Variations of thermal conductivity and HSD of the composites with the Al_2O_3 mass content.

with the increase of nano γ-Al_2O_3 content due to the low thermal conductivity of nano γ-Al_2O_3, which is about 0.3 W (m K)$^{-1}$. The porosity of the initial material is the largest under the same reaction environment and the thermal conductivity is the lowest. Due to the thermal conductivity measurement was conducted immediately after the drying treatment, it can be considered that there was no water present in the composites. Therefore, the data obtained can reflect the thermal conductivity of composite materials during the initial hydration reaction. On the other hand, the HSD of composites (30 °C and 80% RH for 1 h hydration) increases along with the γ-Al_2O_3 ratio, demonstrating that the addition of nano γ-Al_2O_3 promotes the HSD of composites. The heat and mass transfer are two factors that need to be considered comprehensively for chemical heat storage. From the perspective of heat transfer, it can be seen from Fig. 7 that the optimal γ-Al_2O_3 addition ratio should be less than 5%. However, it also can be found that the rising ratio of HSD and the falling ratio of thermal conductivity become slow with the γ-Al_2O_3 addition ratio of more than 5%. For this study, the optimum addition ratio of γ-Al_2O_3 would be 5–10%. Consequently, there is a trade-off between thermal conductivity and HSD for practical applications.

Activation energy refers to the energy required for a molecule to change from normal to an active state which is prone to chemical reactions. The chemical reaction rate is closely related to the size of the activation energy. The lower the activation energy, the faster the reaction rate. Therefore, studying the value of the activation energy can also effectively reflect the speed of the reaction.[60] The activation energy of dehydration performance of LiCl and LiCl·H_2O-Al_2O_3-15% were calculated by Ozawa method[61] for computing the activation energy of thermal decomposition and dehydration reaction.[62] According to Ozawa method, the following equation can be obtained:

$$\ln\left(\frac{\beta}{T^2}\right) = \ln\frac{R}{E}\frac{A}{f(\alpha)} - \frac{E}{R}\frac{1}{T} \quad (13)$$

E is activation energy [kJ mol^{-1}], the value of heating rate (β) is 3, 5, 7 and 10 [K (min)$^{-1}$], T is temperature [K], the value of R is

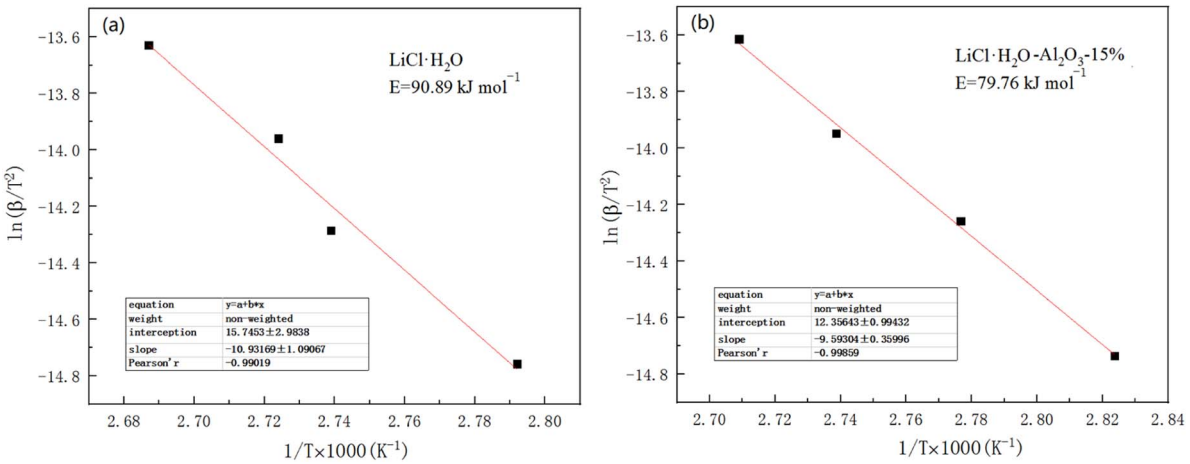

Fig. 8 The activation energy of dehydration reaction of (a) LiCl·H_2O, (b) LiCl·H_2O-Al_2O_3-15%.

8.314 [J (mol K)$^{-1}$], A is the pre-exponential factor, α is the dehydration conversion and $f(\alpha)$ is the function of dehydration conversion. During the calculation of activation energy, the dehydration conversion kept constant at 70%.[61,62] As shown in Fig. 8, the activation energy of dehydration reaction for LiCl and LiCl·H_2O-Al_2O_3-15% is 90.89 kJ mol^{-1} and 79.76 kJ mol^{-1}, respectively. It can be found that the addition of Al_2O_3 is useful for decreasing the activation energy of composites. It is speculated that the addition of γ-Al_2O_3 provides more loading area for LiCl, so that LiCl can absorb more water vapor in the same test environment and time to promote hydration reaction. And –AlCl bond is formed after the reaction of LiCl with γ-Al_2O_3, which reduces the activation energy of dehydration reaction.[54]

4 Conclusions

In this study, the LiCl·H_2O-Al_2O_3 composites were successfully constructed and characterized. The structural properties of these composites was experimentally investigated by XRD, SEM, BET, *in situ* DRIFT spectroscopy and the thermal performance were obtained by TG-DSC and a hot disk thermal constant analyzer. The following findings can be addressed:

(1) Results of XRD show that a complex of $LiAlOCl_2$ was formed by LiCl·H_2O and Al_2O_3. Moreover, with the increase of γ-Al_2O_3 content, the particle size of LiCl·H_2O-Al_2O_3 composites gradually decreased and became uniform through TEM graphs.

(2) According to the *in situ* DRIFT spectroscopy results, the addition of Al_2O_3 accelerated the hydration rate of the material, concentrated the utilization range of spectrum, and promoted the desorption of physical adsorbed H_2O and low-frequency structural –OH in the materials. Furthermore, LiCl-Al_2O_3-20% exhibited the highest specific surface area (15.18 m^2 g^{-1}), which is 34.5 times higher than that of pure LiCl.

(3) Compared with pure LiCl·H_2O, LiCl·H_2O-Al_2O_3 composites exhibited better thermal storage performance, higher HSD of LiCl·H_2O monomer (714.7 kJ kg^{-1}) and water uptake (0.26 g g^{-1}). Meanwhile, the desorption temperature of composites decreased compared with that of the pure LiCl and the addition of Al_2O_3 is useful for decreasing the activation energy of composites (90.89 kJ mol^{-1} to 79.76 kJ mol^{-1}). However, the thermal conductivity of composite decreased with the increase of nano γ-Al_2O_3 content. Further research should be undertaken to improve this aspect.

Conflicts of interest

There are no conflicts to declare.

Acknowledgements

The authors gratefully acknowledge financial support from the National Natural Science Foundation of China (no. 52176091 and no. 52006158), and the Open Fund of Science and Technology on Thermal Energy and Power Laboratory (no. TPL2020A02). We would also like to acknowledge Juan Fu from GuangZhou Institute of Energy Conversion for the experimental guidance.

References

1 , Global Temperature–Latest Annual Average Anomaly (2020) Global Climate Change, https://climate.nasa.gov/vital-signs/global-temperature/.
2 C. Haddad, C. Périlhon, A. Danlos, M.-X. François and G. Descombes, Some efficient solutions to recover low and medium waste heat: competitiveness of the thermoacoustic technology, *Energy Procedia*, 2014, **50**, 1056–1069, DOI: 10.1016/j.egypro.2014.06.125.
3 M. R. Biradar, S. V. Bhosale, P. P. Morajakar and S. V. Bhosale, A review on energy storage devices based on rylene imide dyes: Synthesis, applications and challenges, *Fuel*, 2022, **310**, 122487, DOI: 10.1016/j.fuel.2021.122487.
4 C. Che and Y. Yin, Improvement of low-grade heat utilization: Sensitivity mechanism of saturated vapor pressure–temperature in dehumidified materials, *Appl. Therm. Eng.*, 2023, **230**, 120788, DOI: 10.1016/j.applthermaleng.2023.120788.
5 M. Papapetrou, G. Kosmadakis, A. Cipollina, U. L. Commare and G. Micale, Industrial waste heat: estimation of the technically available resource in the EU per industrial sector, temperature level and country, *Appl. Therm. Eng.*, 2018, **138**, 207–216, DOI: 10.1016/j.applthermaleng.2018.04.043.
6 M. Yu, X. Liu, Z. Liu and S. Yang, Energy, exergy, economic and environmental (4E) analysis of a novel power/refrigeration cascade system to recover low-grade waste heat at 90–150 °C, *J. Cleaner Prod.*, 2022, **363**, 132353, DOI: 10.1016/j.jclepro.2022.132353.
7 S. Daniarta, M. Nems and P. Kolasinski, A review on thermal energy storage applicable for low- and medium- temperature organic Rankine cycle, *Energy*, 2023, **27**, 127931, DOI: 10.1016/j.energy.2023.127931.
8 R. K. Sambare, S. Joshi and N. C. Kanojiya, Improving the freshwater production from tubular solar still using sensible heat storage materials, *Therm. Sci. Eng. Prog.*, 2023, **38**, 101676, DOI: 10.1016/j.tsep.2023.101676.
9 S. Yu, D. Han, W. He, M. Zhou, L. Zhu, Y. Gao, G. Cui and T. Peng, Analysis and optimization of transient heat dissipation characteristics of high power resistors with a sensible heat storage method, *Appl. Therm. Eng.*, 2023, **226**, 120246, DOI: 10.1016/j.applthermaleng.2023.120246.
10 Y. B. Tao and Y. L. He, A review of phase change material and performance enhancement method for latent heat storage system, *Renewable Sustainable Energy Rev.*, 2018, **93**, 245–259, DOI: 10.1016/j.rser.2018.05.028.
11 V. V. Upadhyay and S. Singhal, A review of current developments in the use of materials with latent heat phase changes for the storage of thermal energy, *Mater. Today*, 2023, 4, DOI: 10.1016/j.matpr.2023.02.187.
12 J. Lin, Q. Zhao, H. Huang, H. Mao, Y. Liu and Y. Xiao, Applications of low-temperature thermochemical energy storage systems for salt hydrates based on material classification: A review, *Sol. Energy*, 2021, **214**, 149–178, DOI: 10.1016/j.solener.2020.11.055.

13 K. E. N'Tsoukpoe, G. Restuccia, T. Schmidt and X. Py, The size of sorbents in low pressure sorption or thermochemical energy storage processes, *Energy*, 2014, **77**, 983–998, DOI: 10.1016/j.energy.2014.10.013.

14 W. Hua, H. Yan, X. Zhang, X. Xu, L. Zhang and Y. Shi, Review of salt hydrates-based thermochemical adsorption thermal storage technologies, *J. Energy Storage*, 2022, **56**, 106158, DOI: 10.1016/j.est.2022.106158.

15 Z. Chen, Y. Zhang, Y. Zhang, Y. Su and S. Riffat, A study on vermiculite-based salt mixture composite materials for low-grade thermochemical adsorption heat storage, *Energy*, 2023, **30**, 127986, DOI: 10.1016/j.energy.2023.127986.

16 J. T. Chen, B. Q. Xia and C. Y. Zhao, Topology optimization for heat transfer enhancement in thermochemical heat storage, *Int. J. Heat Mass Transfer*, 2020, **154**, 119785, DOI: 10.1016/j.ijheatmasstransfer.2020.119785.

17 S. Wu, T. X. Li, T. Yan and R. Z. Wang, Advanced thermochemical resorption heat transformer for high-efficiency energy storage and heat transformation, *Energy*, 2019, **175**, 1222–1233, DOI: 10.1016/j.energy.2019.03.159.

18 H. Böhm and J. Lindorfer, Techno-economic assessment of seasonal heat storage in district heating with thermochemical materials, *Energy*, 2019, **179**, 1246–1264, DOI: 10.1016/j.energy.2019.04.177.

19 A. U. Rehman, T. Zhao, I. Muhammad, S. Rasheed, R. Shah, A. R. Altaf, F. Zhang and S. Yun, $MgCl_2$-MXene based nanohybrid composite for efficient thermochemical heat storage application, *J. Energy Storage*, 2023, **59**, 106509, DOI: 10.1016/j.est.2022.106509.

20 T. Yan and H. Zhangr, A critical review of salt hydrates as thermochemical sorption heat storage materials: Thermophysical properties and reaction kinetics, *Sol. Energy*, 2022, **242**, 157–183, DOI: 10.1016/j.solener.2022.07.002.

21 T. Yan, Z. H. Kuai and S. F. Wu, Multi-mode solid-gas thermochemical resorption heat transformer using $NiCl_2$-$SrCl_2/NH_3$, *Appl. Therm. Eng.*, 2020, **167**, 114800, DOI: 10.1016/j.applthermaleng.2019.114800.

22 T. Yan, R. Z. Wang and T. X. Li, Experimental investigation on thermochemical heat storage using manganese chloride/ammonia, *Energy*, 2018, **143**, 562–574, DOI: 10.1016/j.energy.2019.07.105.

23 J. Fitó, A. Coronas, S. Mauran, N. Mazet, M. Perier-Muzet and D. Stitou, Hybrid system combining mechanical compression and thermochemical storage of ammonia vapor for cold production, *Energy Convers. Manage.*, 2019, **180**, 709–723, DOI: 10.1016/j.enconman.2018.11.019.

24 A. Gordeeva, S. Strelova, L. Gordeeva and Y. Aristov, "LiCl/vermiculite – Methanol" as working pair for adsorption heat storage: Adsorption equilibrium and dynamics, *Energy*, 2019, **186**, 0360–5442, DOI: 10.1016/j.energy.2019.07.105.

25 R. Xie, J. Sun, Y. Shi and J. Wei, Baffled-type thermochemical reactor for high-efficient hydrogen production by methanol steam reforming, *Int. J. Hydrogen Energy*, 2023, **48**(61), 23425–23439, DOI: 10.1016/j.ijhydene.2023.03.166.

26 K. S. Babu, E. A. Kumar and S. S. Murthy, Thermochemical energy storage using coupled metal hydride beds of Mg-$LaNi_5$ composites and LaNi5 based hydrides for concentrated solar power plants, *Appl. Therm. Eng.*, 2023, **219**, 119521, DOI: 10.1016/j.applthermaleng.2022.119521.

27 Y. Zhao, C. Y. Zhao, C. N. Markides, H. Wang and W. Li, Medium- and high-temperature latent and thermochemical heat storage using metals and metallic compounds as heat storage media: A technical review, *Appl. Energy*, 2020, **280**, 115950, DOI: 10.1016/j.apenergy.2020.115950.

28 J. Cot-Gores, A. Castell and L. F. Cabeza, Thermochemical energy storage and conversion: a state of the art review of the experimental research under practical conditions, *Renewable Sustainable Energy Rev.*, 2012, **16**, 5207–5224, DOI: 10.1016/j.rser.2012.04.007.

29 H. A. Ousaleh, S. Sair, S. Mansouri, Y. Abboud, M. Zahouily, A. Faik and A. E. I. Bouari, Enhanced inorganic salts stability using bentonite clay for high-performance and low-cost thermochemical energy storage, *J. Energy Storage*, 2022, **49**, 104140, DOI: 10.1016/j.est.2022.104140.

30 L. Calabrese, D. Palamara, E. Piperopoulos, E. Mastronardo, C. Milone and E. Proverbio, Deviceful LiCl salt hydrate confinement into a macroporous silicone foam for low-temperature heat storage application, *J. Sci.: Adv. Mater. Devices*, 2022, **7**, 100463, DOI: 10.1016/j.jsamd.2022.100463.

31 V. Brancato, L. G. Gordeeva, A. L. Sapienza, V. Palomba, S. Vasta, A. D. Grekova, A. Frazzica and Y. I. Aristov, Experimental characterization of the LiCl/vermiculite composite for sorption heat storage applications, *Int. J. Refrig.*, 2019, **105**, 92–100, DOI: 10.1016/j.ijrefrig.2018.08.006.

32 G. Whiting, D. Grondin, S. Bennici and A. Auroux, Heats of water sorption studies on zeolite-$MgSO_4$ composites as potential thermochemical heat storage materials, *Sol. Energy Mater. Sol. Cells*, 2013, **112**, 112–119, DOI: 10.1016/j.solmat.2013.01.020.

33 A. D. Grekova, L. G. Gordeeva, Z. Lu, R. Wang and Y. I. Aristov, Composite "LiCl/MWCNT" as advanced water sorbent for thermal energy storage: Sorption dynamics, *Sol. Energy Mater. Sol. Cells*, 2018, **176**, 273–279, DOI: 10.1016/j.solmat.2017.12.011.

34 X. Ke and V. A. Baki, Assessing the suitability of alkali-activated metakaolin geopolymer for thermochemical heat storage, *Sol. Energy Mater. Sol. Cells*, 2021, **325**, 111329, DOI: 10.1016/j.micromeso.2021.111329.

35 N. Yu, R. Z. Wang, Z. S. Lu and L. W. Wang, Study on consolidated composite sorbents impregnated with LiCl for thermal energy storage, *Int. J. Heat Mass Transfer*, 2015, **84**, 660–670, DOI: 10.1016/j.ijheatmasstransfer.2015.01.065.

36 X. Zheng and R. Z. Wang, Microstructure and sorption performance of consolidated composites impregnated with LiCl, *Int. J. Refrig.*, 2019, **98**, 452–458, DOI: 10.1016/j.ijrefrig.2018.11.031.

37 J. Aarts, B. V. Ravensteijn, H. Fischer, O. Adan and H. Huinink, Polymeric stabilization of salt hydrates for thermochemical energy storage, *Appl. Energy*, 2023, **341**, 121068, DOI: 10.1016/j.apenergy.2023.121068.

38 X. Zheng, T. S. Ge, Y. Jiang and R. Z. Wang, Experimental study on silica gel-LiCl composite desiccants for desiccant

coated heat exchanger, *Int. J. Refrig.*, 2015, **51**, 24–32, DOI: 10.1016/j.ijrefrig.2014.11.015.

39 L. Z. Zhang, Y. Y. Wang, C. L. Wang and H. Xiang, Synthesis and characterization of a PVA/LiCl blend membrane for air dehumidification, *J. Membr. Sci.*, 2008, **308**, 198–206, DOI: 10.1016/j.memsci.2007.09.056.

40 H. Zhao, Z. Wang, Q. Li, T. Wu, M. Zhang and Q. Shi, Water sorption on composite material "zeolite 13X modified by LiCl and $CaCl_2$", *Microporous Mesoporous Mater.*, 2020, **299**, 110109, DOI: 10.1016/j.micromeso.2020.110109.

41 Y. N. Zhang, R. Z. Wang and T. X. Li, Thermochemical characterizations of high-stable activated alumina/LiCl composites with multistage sorption process for thermal storage, *Energy*, 2018, **156**, 240–249, DOI: 10.1016/j.energy.2018.05.047.

42 D. G. Gunjo, S. R. Jena, P. Mahanta and P. S. Robi, Melting enhancement of a latent heat storage with dispersed Cu, CuO and Al_2O_3 nanoparticles for solar thermal application, *Renewable Energy*, 2018, **121**, 652–665, DOI: 10.1016/j.renene.2018.01.013.

43 H. Sun, Y. Li, X. Yan, J. Zhao and Z. Wang, Thermochemical energy storage performance of Al_2O_3/CeO_2 co-doped CaO-based material under high carbonation pressure, *Appl. Energy*, 2020, **263**, 114650, DOI: 10.1016/j.apenergy.2020.114650.

44 M. Bahari, B. Najafi and A. Babapoor, Evaluation of α-AL_2O_3-PW nanocomposites for thermal energy storage in the agro-products solar dryer, *J. Energy Storage*, 2020, **28**, 101181, DOI: 10.1016/j.est.2019.101181.

45 X. Lao, X. Xu, H. Cheng, H. Liu and L. Liang, Effect of rare-earth oxides on microstructure and thermal shock resistance of Al_2O_3-SiC_w composite ceramics for solar thermal storage, *Ceram. Int.*, 2019, **45**, 2003–2011, DOI: 10.1016/j.ceramint.2018.10.098.

46 W. Miao, Y. Wang, X. Li, S. Gan, Y. Lv and Z. Liu, Development of spherical α-Al_2O_3-based composite phase change materials (PCMs) and its utilization in thermal storage building materials, *Thermochim. Acta*, 2019, **676**, 177–185, DOI: 10.1016/j.tca.2019.04.010.

47 S. Bahou, H. Labrim, M. Lakhal, M. Bhihi, B. Hartiti and H. Ez-Zahraouy, Improving desorption temperature and kinetic properties in MgH_2 by vacancy defects: DFT study, *Int. J. Hydrogen Energy*, 2020, **45**(18), 10806–10813, DOI: 10.1016/j.ijhydene.2020.02.024.

48 H. Wu, P. Trens, B. Fraisse, F. Salles and J. Zajac, Hydration mechanism in Ce-exchanged zeolites and heat release performances upon adsorption of water vapour in support of their potential use in thermochemical storage of energy under mild conditions of adsorbent regeneration and saturation, *Microporous Mesoporous Mater.*, 2020, **296**, 109999, DOI: 10.1016/j.micromeso.2020.109999.

49 K. M. Kim, H. T. Oh, S. J. Lim, K. Ho, Y. Park and C. H. Lee, Adsorption equilibria of water vapor on zeolite 3A, zeolite 13X, and dealuminated Y zeolite, *J. Chem. Eng.*, 2016, **61**, 1547–1554, DOI: 10.1021/acs.jced.5b00927.

50 S. P. Weng, *Fourier transform infrared spectrometer*, Chemical Industry Press, 2005, https://max.book118.com/html/2019/0724/8043041133002036.shtm.

51 G. Hambitzer, J. Heitbaum, C. Dambach, M. Kampa, C. Pszolla and C. Ripp, *Rechargeable electrochemical cell*, *US pat.* 20140113182, 2014-04-24, http://www.patentsencyclopedia.com/app/20140113182.

52 D. H. Zhou, *Lithium industry*, Chemical Industry Press, 1996.

53 W. Y. Xu, C. J. Yao, Y. C. Xu and S. G. Hong, Preparation of dimethyldichlorosilane by catalytic disproportionation of $LiAlCl_4/\gamma$-Al_2O_3, *J. Zhengzhou Univ.*, 2017, **38**, 92–96, DOI: 10.13705/j.issn.1671-6833.2017.06.014.

54 L. Zhao, X. Y. Li, C. Hao and C. L. Raston, SO_2 adsorption and transformation on calcined NiAl hydrotalcite-like compounds surfaces: An *in situ* FTIR and DFT study, *Appl. Catal., B*, 2012, **117–118**, 339–345, DOI: 10.1016/j.apcatb.2012.01.034.

55 T. Szabo, O. Berkesi, P. Forgo, K. Josepovits, Y. Sanakis, D. Petridis and I. Dekany, Evolution of surface functional groups in a series of progressively oxidized graphite oxides, *Chem. Mater.*, 2006, **18**, 2740–2749, DOI: 10.1021/cm060258+.

56 L. Vradmana, M. V. Landaub, D. Kantorovich, Y. Koltypin and A. Gedanken, Evaluation of metal oxide phase assembling mode inside the nanotubular pores of mesostructured silica, *Microporous Mesoporous Mater.*, 2005, **79**(1–3), 307–318, DOI: 10.1016/j.micromeso.2004.11.023.

57 L. G. Gordeeva, A. Freni, T. A. Krieger, G. Restuccia and Y. I. Aristov, Composites "lithium halides in silica gel pores": Methanol sorption equilibrium, *Microporous Mesoporous Mater.*, 2008, **112**(1–3), 254–261, DOI: 10.1016/j.micromeso.2007.09.040.

58 H. Zhao, M. Lei, T. Liu, T. Huang and M. Zhang, Synthesis of composite material HKUST-1/LiCl with high water uptake for water extraction from atmospheric air, *Inorg. Chim. Acta*, 2020, **511**, 119842, DOI: 10.1016/j.ica.2020.119842.

59 B. X. Wang, L. P. Zhou and X. F. Peng, Surface and size effects on the specific heat capacity of nanoparticles, *Int. J. Thermophys.*, 2006, **27**, 139–151, DOI: 10.1007/s10765-006-0022-9.

60 H. Zou, F. Evrendilek, J. Liu and M. Buyukada, Combustion behaviors of pileus and stipe parts of Lentinus edodes using thermogravimetric-mass spectrometry and Fourier transform infrared spectroscopy analyses: thermal conversion, kinetic, thermodynamic, gas emission and optimization analyses, *Bioresour. Technol.*, 2019, **288**, 121481, DOI: 10.1016/j.biortech.2019.121481.

61 M. Kubota, S. Matsumoto, H. Matsuda, H. Y. Huang, Z. H. He and X. X. Yang, Chemical heat storage with LiOH/$LiOH \cdot H_2O$ reaction for low-temperature heat below 373 K, *Adv. Mater. Res.*, 2014, **953–954**, 757–760, DOI: 10.4028/www.scientific.net/AMR.953-954.757.

62 S. Li, H. Huang, X. Yang, Y. Bai, J. Li, N. Kobayashi and M. Kubota, Hydrophilic substance assisted low temperature $LiOH \cdot H_2O$ based composite thermochemical materials for thermal energy storage, *Appl. Therm. Eng.*, 2018, **128**, 706–711, DOI: 10.1016/j.applthermaleng.2017.09.050.